Ceramics International xxx (xxxx) xxx–xxx

Contents lists available at ScienceDirect

Ceramics International

journal homepage: www.elsevier.com/locate/ceramint

Low (and negative) thermal expansion Al_2TiO_5 materials and Al_2TiO_5 - $3Al_2O_3.2SiO_2$ - $ZrTiO_4$ composite materials. Processing, initial zircon proportion effect, and properties

M.A. Violini[a,b,*], M.F. Hernández[a,b], M. Gauna[a], G. Suarez[a,b], M.S. Conconi[a,b], N.M. Rendtorff[a,b,*]

[a] CETMIC, Centro de Tecnología de Recursos Minerales y Cerámica (CONICET La Plata - CIC PBA), Camino Centenario y 506, C.C. 49, (B1897ZCA), M.B. Gonnet, Buenos Aires, Argentina

[b] Depto. de Química, Facultad de Ciencias Exactas, Universidad Nacional de La Plata, 47 y 115, La Plata, Buenos Aires, Argentina

ARTICLE INFO

Keywords:
Aluminum titanate
Structural ceramics
Composite ceramics
Low thermal expansion ceramics
Processing, properties

ABSTRACT

Aluminum titanate (Al_2TiO_5) materials and aluminum titanate - mullite- zirconium titanate (Al_2TiO_5 - $3Al_2O_3.2SiO_2$ - $ZrTiO_4$) composite materials were successfully processed from fine commercial powders and characterized. This was achieved by zircon ($ZrSiO_4$) addition to stoichiometric alumina - titania mixtures. Zircon addition was the principal processing variable explored. This additive stabilizes the unstable aluminum titanate phase, enhances the sintering process, restricts microcrack development and improves the mechanical properties of the bulk material, but has a slight detrimental effect on its thermal expansion behavior (α_{app} from -1.5 to $2.5 \times 10^{-6}\,°C^{-1}$ in the RT-800 °C range). With a clear microstructure configuration change, all the technological properties are directly (linearly) correlated with zircon proportion in the initial formulation in the range between 5 and 30 wt%.

Developed phases were established, relatively dense ceramics were produced, and complex microstructures with multiphasic interlocked grains were identified. Also, an interconnected microcrack matrix was observed with no material integrity loss which explained the low or even negative thermal expansion behaviors observed in the developed materials. This, together with the mechanical behavior detected, encourages structural applications with high thermomechanical solicitations.

The triplex composite material presented an excellent thermomechanical behavior and low porosity, 48 MPa flexural strength, low stiffness and high sintering grade with low thermal expansion.

1. Introduction

Nowadays, composite materials have an important industrial and technological development. The manufacturer's capability to achieve the desired properties and behaviors is enhanced by combining two or more different materials; however, the final properties are not necessarily between those of pure materials [1–6]. In the manufacture of structural ceramics, the composite ceramic-ceramic strategy has been used for decades [5,7–9]. Once the constituent phases and the processing conditions are chosen, the phase proportion becomes one of the most important processing variables [10].

Low, null or negative thermal expansion ceramic materials have drawn attention for several decades [11–14]; and proposed for high thermomechanical demand applications.

Aluminum titanate (AT = Al_2TiO_5) is a material with a very low thermal expansion coefficient, excellent thermal shock resistance, very low thermal conductivity (approximately 1.5 $W\,m^{-1}\,K^{-1}$) and high melting point (about 1860°C). These properties make it suitable for applications where thermal insulation and thermal shock resistance are required [15–25]. However, its applications are restricted because it decomposes in the temperature range 800 – 1280°C and it has very low fracture strength due to the extensive microcracking [26–28].

Different strategies to stabilize Al_2TiO_5 have been studied. One of them is the of Al_2TiO_5 grain growth through the addition of additives such as SiO_2, ZrO_2, mullite and $ZrTiO_4$ [17,25]. The amount of addition of these second phases is dissimilar. Moreover, composite multiphasic materials have been successfully processed [11], but, in some cases, systematic studies have not been reported.

The mullite (M – $3Al_2O_3.2SiO_2$) ceramics have had and will continue to have a significant role in the development of traditional and

* Corresponding authors at: CETMIC, Centro de Tecnología de Recursos Minerales y Cerámica (CONICET La Plata - CIC PBA), Camino Centenario y 506, C.C. 49, B1897ZC M.B. Gonnet, Buenos Aires, Argentina.

E-mail addresses: aviolini@cetmic.unlp.edu.ar (M.A. Violini), rendtorff@cetmic.unlp.edu.ar (N.M. Rendtorff).

https://doi.org/10.1016/j.ceramint.2018.08.208
Received 2 July 2018; Received in revised form 8 August 2018; Accepted 19 August 2018

advanced ceramics [20,29–32]. Mullite is the only stable crystalline phase in the aluminosilicate system, under normal atmospheric pressure at room through elevated temperatures. Its chemical composition ranges from $3Al_2O_3$–$2SiO_2$ to approximately $2Al_2O_3$–SiO_2. It has received significant attention during the last decades as a potential structural material for high-temperature applications. Mullite-based composite structural ceramics have particularly been developed [7,10,29,30].

Zirconium titanate (ZT = $ZrTiO_4$) is commonly used as a dielectric in microwave devices due to its high permittivity at microwave frequencies [33–35]. ZT has been proposed for severe structural and thermomechanical applications [36,37] and is a well-known compound in the field of electroceramics, as constituent of dielectric resonators and components for telecommunications [38].

Some materials from the ZrO_2–Al_2O_3–SiO_2–TiO_2 quaternary system have been studied by other authors. Particularly, the phase diagram has been reported and discussed [39], and the transient liquid phase sintering mechanism has been confirmed. Recently, we studied a family of composites of the same quaternary system with a continuous-dispersed phase microstructural configuration. Particularly, the studied material presented mullite as the continuous phase, and zirconia together with zirconium titanate as dispersed phases [7]. In that work, alumina, zircon and titania were chosen as starting powders in a 3:2:1 M ratio. Both sintering and reaction occurred after the thermal treatments. The reaction progress and densification evolutions were established. Dense triplex composite materials were achieved after 1500 °C treatments. Aluminum titanate (Al_2TiO_5) was found to be an intermediate of the reaction after 1400 °C treatments. As mentioned, due to its low cost and availability, the starting powders chosen in that work were alumina, zircon and titania, which are also employed in this work.

Pure aluminum titanate is not thermally stable [40]; hence pure aluminum titanate material was not studied. In this work, we aim to study and compare two microstructural configurations: an aluminum titanate-based material relatively dense and a composite material with aluminum titanate as continuous phase with mullite and zirconium titanate as dispersed phases. They would be achieved after thermal treatments of compacted powders with different additions of zircon (5, 15 and 30 wt%) to a stoichiometric alumina – titania mixture. This would occur by the combination of several thermal reactions, shown in Eqs. (1–4):

$$Al_2O_3 + TiO_2 \rightarrow Al_2TiO_5 \quad (1)$$

$$ZrSiO_4 \rightarrow ZrO_2 + SiO_2 \quad (2)$$

$$3Al_2O_3 + 2SiO_2 \rightarrow 3Al_2O_3.2SiO_2 \quad (3)$$

$$ZrO_2 + TiO_2 \rightarrow ZrTiO_4 \quad (4)$$

The objective of the present work is to study the reaction-sintering process, the developed crystalline phases and microstructures together with the mechanical properties of the final materials. This will shed light on the material and microstructure design of this composite materials family.

2. Experimental procedure

2.1. Starting materials and processing

The commercial starting powders employed were Al_2O_3 (α-alumina A-16SG, Alcoa Inc., USA), TiO_2 (Titanium (IV) oxide, Cicarelli) 95% anatase-5% rutile and $ZrSiO_4$ (Zircon KREUTZONIT® Super Extra Weiß, Helmut Kreutz Mahlwerke GmbH).

Three equimolar mixtures of Al_2O_3 and TiO_2 with different percentages of $ZrSiO_4$ were studied: ATZ5 (5 wt% $ZrSiO_4$ initial content), ATZ15 (15 wt% $ZrSiO_4$ initial content) and ATZ30 (30 wt% $ZrSiO_4$ initial content).

An initial mixture was prepared in a Fritsch Pulverisette 7 planetary ball mill, with isopropyl alcohol, performing 5 cycles of 2 min at 500 rpm, with one minute of pause between cycles. 85 ml zirconia jars with 10 mm zirconia balls were employed. The mixed slurry was dried and sieved through a 100-mesh screen. The samples were shaped by uniaxial pressing at 50 MPa. Thus, $20 \times 3 \times 3\ mm^3$ prismatic probes were obtained. These probes were fired in an electric furnace with a heating rate of 5 °C/min up to 1500 °C with 2 h soaking and cooling at 10 °C/min down to 300 °C. The maximum temperature was chosen after a dilatometric study, taking into account previous reports [39,41].

2.2. Characterization

The reaction sintering was followed by simultaneous thermogravimetric (TG) and differential thermal analyses (DTA) of the unfired mixtures. Both thermal analyses were carried out simultaneously, at a 5 °C/min heating rate up to 1450 °C, in air atmosphere (TG-DTA Rigaku Evo plus II, Japan). In addition, a dilatometric analysis (DA) of the unfired mixtures was carried out, using a reversible program with a 5 °C/min heating rate up to 1450 °C and 10 °C/min cooling rate up to 300 °C, in air atmosphere (TMA Rigaku Evo plus II, Japan) [7,42].

Then, the materials obtained after sintering were characterized. The identification and quantification of crystalline phases were carried out by X-ray diffraction (XRD) (Philips 3020 with Cu-kα radiation, Ni filter, at 40 kV-35 mA). The XRD patterns were analyzed with the program FullProf (3.0 version, June 2015), which is a multipurpose profile-fitting program, including Rietveld refinement to perform phase quantification [43,44]. The apparent density and open porosity were determined by the Archimedes method in water. The distribution and size of the pores obtained were evaluated by mercury intrusion porosimetry, using a mercury porosimeter (Thermo Scientific Pascal 440 Series. The microstructure analysis was carried out by scanning electron microscopy (SEM) (JEOL, JCM −6000) and afterwards an EDS analysis (EDAX- JEOL), was performed.

The mechanical properties of the obtained materials were evaluated. The flexural strength and the static elastic modulus were determined by the three-point bending test in a universal testing machine INSTRON 4483, 18 mm span was employed, and with 0.025 mm/min displacement rate. The dynamic elastic modulus was measured by the impulse excitation technique with a GrindoSonic, Mk5 ''Industrial'' model; at least eight samples were evaluated for each material [45].

Finally, the thermal expansion behavior of the obtained materials was studied by dilatometry using a heating rate of 5 °C/min, in air atmosphere (TMA Rigaku Evo plus II, Japan).

3. Results and discussion

3.1. Thermal behavior and sintering of the studied mixtures

3.1.1. Thermal behavior, differential thermal analysis and thermogravimetry

Fig. 1 shows a section of the DTA curve of the studied mixtures in the range between 1350 and 1425 °C. A negative endothermic peak can be easily observed. This peak could be associated with aluminum titanate formation from aluminum and titanium oxides [41]. In all the cases it can be said that the reaction is complete below 1420 °C. Taking into account the equipment accuracy, it can be stated that the reaction temperature is not affected by zircon addition in the studied range.

3.1.2. Dilatometric analysis

The dilatometric curves (DA) of the three studied mixtures show a shrinkage stage between approximately 900 and 1400 °C. This is associated with the reaction-sintering process of the starting powders. During this process, the formation of Al_2TiO_5, $ZrTiO_4$ and mullite (Eqs. 1–4) occurs, accompanied by the densification of the powders. This occurs through a transient liquid phase, which was previously observed in materials of the same quaternary system [39] that present a eutectic

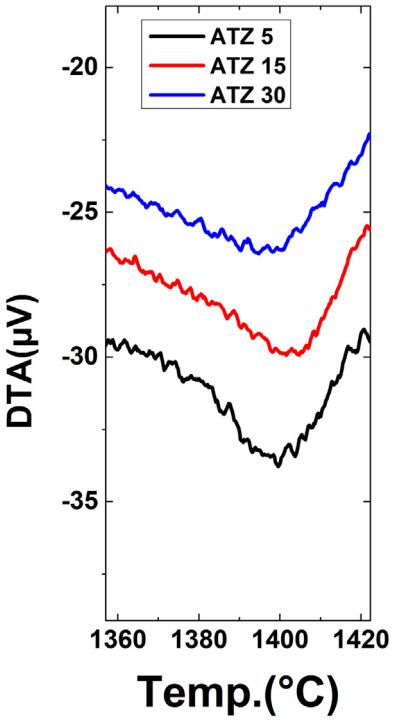

Fig. 1. Section of DTA curves of unfired mixtures; endothermic peaks correspond to Al_2TiO_5 formation.

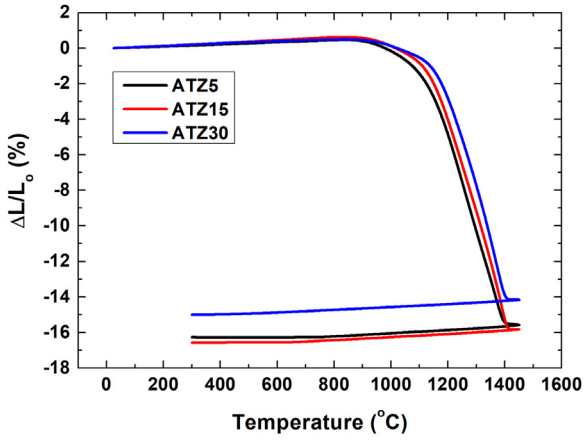

Fig. 2. Dilatometric analysis (DA) of the unfired mixtures.

below 1450 °C [39]. The observed relative shrinkages are 15.9%, 16.4% and 14.7% for samples ATZ5, ATZ15 and ATZ30 respectively.

Based on these two dynamic tests, it was established that the optimum heating cycle is 5 °C/min up to 1500 °C, to ensure complete conversion and maximum sintering.

3.1.3. Textural properties: porosity and density

Fig. 3 shows the evolution of the textural properties (density and porosity) with the initial $ZrSiO_4$ content of the developed materials. These can be taken as sintering parameters. Although some open porosity was observed, the obtained materials can be considered dense ones. Cracks could be understood as pores, and are sometimes unavoidable in aluminum titanate materials [26,27].

The density increased with the initial $ZrSiO_4$ content and the porosity decreased, which indicates that zircon enhances the sintering process. These results are in agreement with previous studies [17,25]. Particularly, Nagano *et al.* established that zircon could be employed for this purpose in aluminum titanate materials obtained by co-

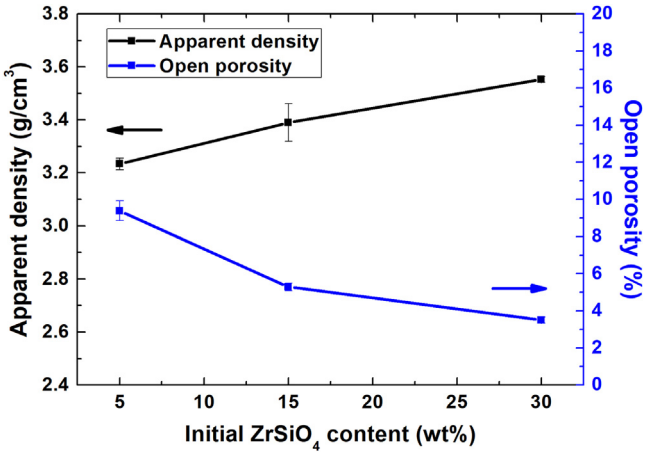

Fig. 3. Apparent density and open porosity of fired samples as a function of the initial $ZrSiO_4$ content.

precipitation, but no zircon content-sintering systematic study was performed.

3.2. Resulting phase compositions

3.2.1. XRD-Rietveld

Diffraction patterns of the studied materials are shown in Fig. 4. The principal crystalline phase is Al_2TiO_5 in all the cases, which is accompanied by $ZrTiO_4$, mullite and a small amount of Al_2O_3. This fact corresponds to the progress of the expected thermochemical processes (Eqs. 1–4). These are in accordance with the phase diagram reported by Melo et al. [39]. The observed total conversion is in agreement with the dilatometric analysis (Fig. 2); the transient liquid phase sintering corresponds to the phases and sintering behavior observed in materials of the same quaternary system. Moreover, the addition of three zircon amounts stabilized the aluminum titanate phase.

The Rietveld refined cell parameters are shown in Table 1. The results are similar to the ones reported in the literature. The alumina cell parameters were not refined because of its low proportion.

Table 2 presents the Rietveld based quantification results and the PDF codes of the identified crystalline phases. Estimated standard deviations are also shown, which were calculated by Fullprof and derived from the estimated standard deviations in individual scale factors for the respective phases, excluding other error contributions. In all the cases the obtained Rwp parameters were satisfactory (below 20). The amount of complementary phases is directly related to the zircon addition, as expected. The small discrepancies with the stoichiometric

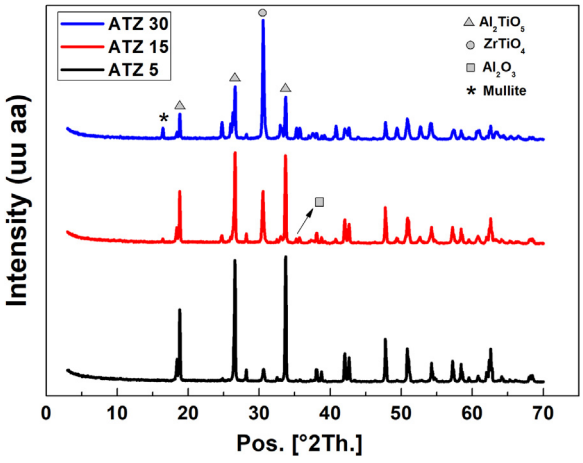

Fig. 4. XRD patterns of the obtained materials, with the main peaks labeled.

Table 1
Cell parameters of the different phases in the three materials. The values were obtained by Rietveld refinement of the DRX patterns.

Al_2TiO_5						
Sample	PDF 00-041-0258					
	Cell parameter					
	a	Error ($x10^{-3}$)	b	Error ($x10^{-3}$)	c	Error ($x10^{-3}$)
ATZ5	9.4356	0.7	9.65214	0.07	3.58791	0.02
ATZ15	9.4371	0.8	9.65741	0.08	3.58641	0.03
ATZ30	9.437	1.0	9.65761	0.09	3.58586	0.03
$ZrTiO_4$						
Sample	PDF 01-080-1783					
	Cell parameter					
	a	Error ($x10^{-3}$)	b	Error ($x10^{-3}$)	c	Error ($x10^{-3}$)
ATZ5	4.776	2.0	5.4500	0.4	5.0230	0.3
ATZ15	4.8162	0.8	5.4291	0.1	5.03149	0.08
ATZ30	4.8037	0.5	5.43019	0.06	5.02687	0.05
Mullite ($3Al_2O_3.2SiO_2$)						
Sample	PDF 01-079-1275					
	Cell parameter					
	a	Error ($x10^{-3}$)	b	Error ($x10^{-3}$)	c	Error ($x10^{-3}$)
ATZ5	–	–	–	–	–	–
ATZ15	7.564	3.0	7.6983	0.3	2.89178	0.07
ATZ30	7.561	1.0	7.6966	0.1	2.89080	0.03
Al_2O_3						
Sample	PDF 01-076-0144					
	Cell parameter					
	a	Error ($x10^{-3}$)	b	Error ($x10^{-3}$)	c	Error ($x10^{-3}$)
ATZ5	4.759	4.0	4.759	4.0	12.982	4.0
ATZ15	4.75792	0.0	4.75792	0.0	12.94009	0.0
ATZ30	–	–	–	–	–	–

Table 2
Results of the Rietveld phase quantification.

Sample	Rwp	Crystalline phases							
		AT Al_2TiO_5		ZT $ZrTiO_4$		M $3Al_2O_3.2SiO_2$		A Al_2O_3	
		wt%	Error	wt%	Error	wt%	Error	wt%	Error
ATZ5	15.4	95.3	0.6	3.2	0.1	–	–	1.5	0.3
ATZ15	15.3	81.1	1.1	11.9	0.2	6.9	0.4	0.2	0.1
ATZ30	19.5	44.7	0.9	28.2	0.9	27.2	0.7	–	–

results can be explained by the uncertainty of the quantification methodology and the possible existence of solid solution, especially in the ZT phase [46–48] and mullite [29]. In fact, the ZT cell parameters vary within the three studied materials.

For a better visualization of the developed materials microstructural configuration, in Fig. 5 the volumetric proportion of the resulting phases for the three studied materials is plotted in pie charts. The apparent open porosity was considered as another phase. Rietveld quantification, Archimedes results and refined cell densities were employed for the construction of these charts. The actual numbers are listed in Table 3.

Evidently, the ATZ5 sample corresponds to an aluminum titanate material and the complementary crystalline phases have an additive role [49]. On the other hand, the ATZ30 sample is clearly a multiphasic composite material with a comparable amount of the three crystalline phases (AT, ZT and M). Finally, the ATZ15 sample is an intermediate between the former two. The small amount of alumina could be explained as unreacted alumina or alumina coming from the aluminum titanate dissociation [40].

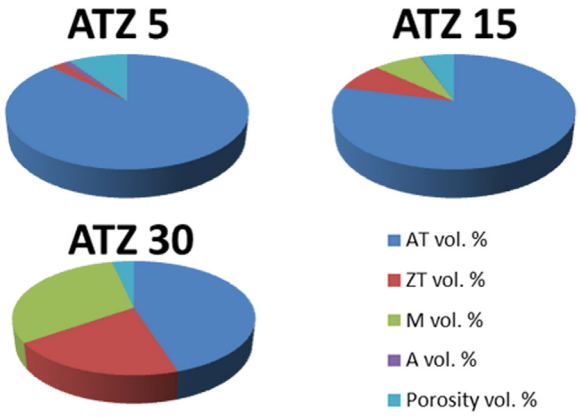

Fig. 5. Volumetric phase proportion of the studied materials.

Table 3
Volumetric phase content of the studied materials.

Sample	Volumetric fraction (%)				
	AT Al_2TiO_5	ZT $ZrTiO_4$	M $3Al_2O_3.2SiO_2$	A Al_2O_3	P Porosity
ATZ5	87.3	2.1	–	1.2	9.4
ATZ15	79.0	8.0	7.6	0.2	5.3
ATZ30	45.0	20.2	31.3	–	3.5

3.3. Microstructure characterization

3.3.1. SEM – EDS

The microstructural characterization consisted of SEM analysis complemented with porosimetric analysis. The SEM analysis was performed both on free fracture surface and diamond paste polished surface, Figs. 6 and 7 respectively. It is well known that due to the anisotropic thermal expansion of Al_2TiO_5 crystals, AT based materials present a microcracked microstructure [17,21,25,27]. The lengths of the cracks are difficult to determine; apparently, they are interconnected as was previously observed in similar materials. However, the integrity was not jeopardized by the crack development during the thermal process due to the addition of zirconium silicate and the mentioned thermal reactions. The presence of round pores can be easily seen in ATZ5, but is not as evident in the other two samples (ATZ15 and ATZ30). The composite strategy for stabilizing and strengthening is the hypothesis of this study.

The typical fracture surface is shown in Fig. 6; cracks (in black) are observed in the three samples. The crack width is below 1 μm; the pore size is higher than 1 μm and visible in ATZ5. At this point, it is difficult to compare the dimension of the crack interconnected matrix. But, apparently, the ATZ5 sample presents a higher amount of cracks, as expected due to the higher amount of AT phase. This fact agrees with the Archimedes results as well.

Fig. 7 depicts SEM images at different magnifications. The samples present some spalling after a long or hard polishing treatment. As mentioned, the materials present an interconnected crack matrix. This effect has been predicted and well reported [24–27].

In the SEM images with lower magnification, the variation of porosity can be easily observed. Some of the apparent pores are a consequence of the mentioned spalling. The sintering is again correlated with the initial zircon proportion. It can be roughly said that the ATZ30 sample presents a larger grain size than the others. In the correctly polished zones the multiphasic microstructure can be observed.

The ATZ30 images show the development of an interlocked polyphasic ceramic microstructure, with ≈ 3–4% of porosity. The phase proportion is as shown in Fig. 5. The sintering process is advanced but

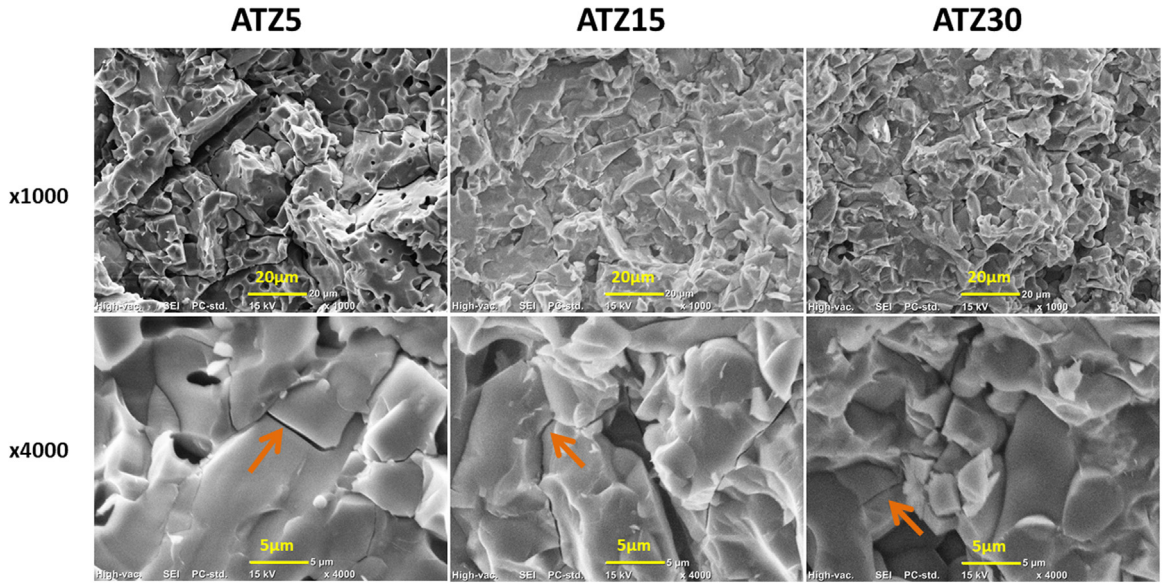

Fig. 6. Free fracture SEM images of the studied materials (x1000 and x4000; upper and lower images respectively); cracks are marked with arrows.

not strictly complete. The grain size is of several microns, and grain shapes are not rounded. Different phases can be delimited. The observed phases correspond to the ones detected by XRD, resulting from the evolution of the mentioned thermal reactions (Eqs. 1–4). Zirconium titanate corresponds to light gray, aluminum titanate to middle gray, and mullite to the darker gray. This was confirmed by local EDS analysis.

3.3.2. Porosimetry

The microstructure presented pores and the developed microcracks; both can be measured by mercury intrusion porosimetry if they are connected to the surface of the material, and are estimated as pores, without any distinction in between. In this technique, pores are assumed to be cylindrical. This fact makes the technique uncertain in these particular cracked materials; however, a comparative analysis was carried out. Fig. 8 shows the cumulative pore distribution (normalized) of the three samples. Table 4 lists the measured percentiles and the plot inset in Fig. 8 presents the pore size distributions. In all the cases the measured pore and crack width are below 1 µm in size. This is of the same order as the starting powder particle size ≈ 0.5, ≈ 0.8 and ≈ 1.0 µm for Al_2O_3, $ZrSiO_4$ and TiO_2 respectively.

Samples ATZ30 and ATZ15 present a sharp peak distribution with modes near the mean pore size (d_{50}). The ATZ30 material presents a narrower pore distribution between 0.08 and below 0.2 µm. The ATZ5 material has a wider and flatter distribution between 0.03 and 0.7 µm. The pore size distribution width follows the ATZ5 > ATZ15 > ATZ30 sequence, which is directly correlated with the open porosity and inverse to the sintering grade. The mean pore size (d_{50}) follows the

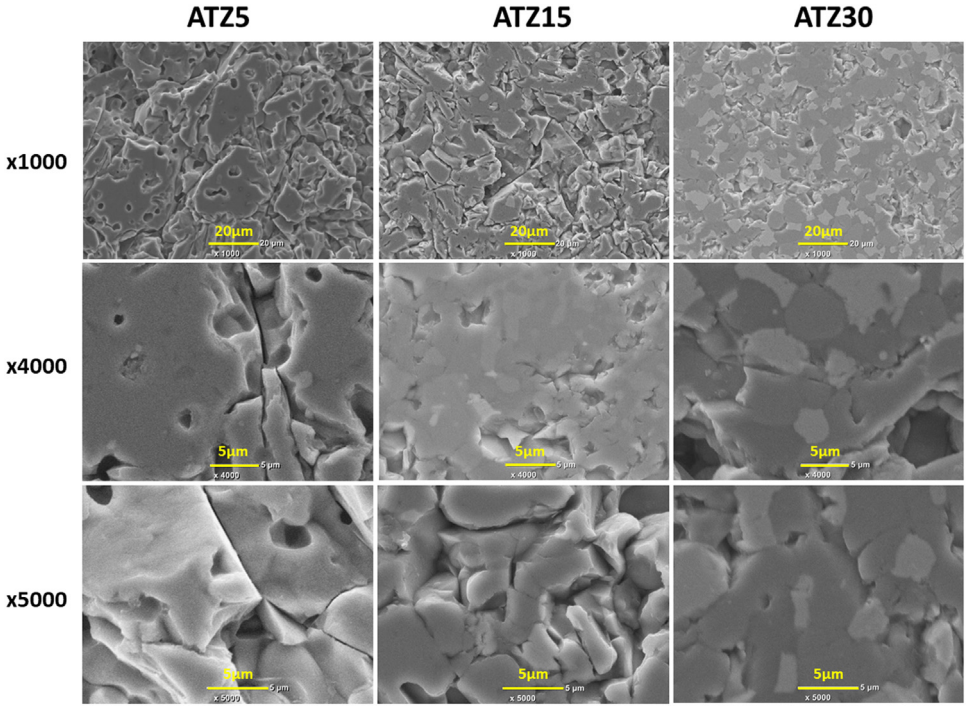

Fig. 7. SEM images of the diamond polished materials at different magnifications (x1000, x4000, x5000).

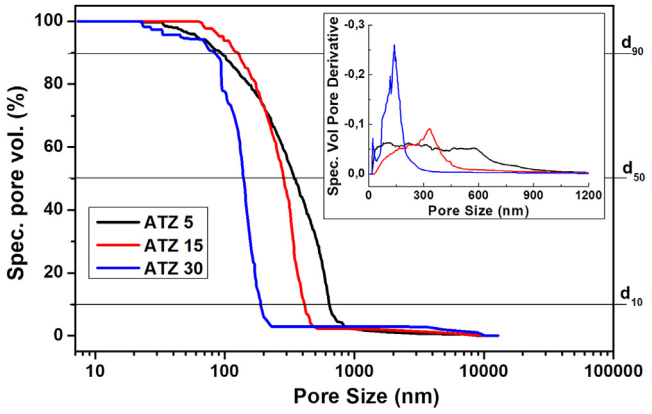

Fig. 8. Open pore size distribution of the obtained materials, measured by mercury intrusion porosimetry; normalized cumulative curves. Pore size distributions are shown in the inset plot.

Table 4
Pore size diameters of the obtained materials.

Sample	d_{10} (μm)	d_{50} (μm)	d_{90} (μm)
ATZ5	0.64	0.35	0.09
ATZ15	0.42	0.29	0.13
ATZ30	0.19	0.14	0.08

inverse sequence, being ATZ5 > ATZ15 > ATZ30. In summary, zircon addition results in a decrease of the open porosity and in a narrower pore distribution.

3.4. Mechanical and thermal behaviors

The mechanical behavior of the materials was studied by two tests, the quasi-static flexural strength and the dynamic elastic modulus by the impulse excitation technique, which provides three mechanical parameters (σ_f, E_{st} and E_d). It is well known that these parameters are strongly related to the microstructure of the developed materials. In this case, the observed microcracks will undoubtedly affect the mechanical parameter values. The actual applicability of the structural materials will be achieved only if the mechanical parameters are appropriate.

The flexural strength (σ_f) values are plotted as a function of the initial zircon proportion in Fig. 9. The σ_f values and dispersions are similar to the one measured in similar AT materials [6,18,25]. The values are evidently correlated with the initial zircon addition; higher zircon content results in a higher σ_f.

Furthermore, the static and dynamic Young modulus (E_{st} and E_d, respectively) are plotted in Fig. 9. The measured young moduli are also clearly correlated with the zircon addition proportion. The values are remarkably lower than in other structural dense ceramics, but similar to those of other AT based materials [18,28]. It is worth pointing out that the difference between the static and dynamic values (1:5) is clear evidence of the presence of cracks in the microstructure [50].

In general, the composite configuration (ATZ30) presents better mechanical behavior. Moreover, the ATZ5 material value is below some structural requirements, but is comparable to that obtained in previous reports [17,18].

The mechanical behavior is proportional to the zircon addition. This can be explained by the higher sintering and the lower microcrack developments previously described, showing that the zircon addition stabilizes and strengthens the aluminum titanate ceramics.

These results encourage the structural applications of these materials

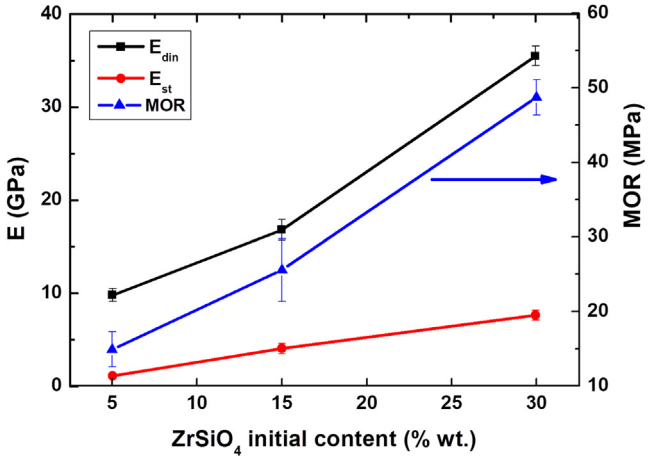

Fig. 9. Flexural strength (σ_f), static and dynamic elastic moduli (E_d and E_{st}), as a function of the initial $ZrSiO_4$ content.

3.4.1. Dilatometric behavior up to 800 °C

The combination of mechanical and thermomechanical properties found in materials of this kind supports their utilization for linings and components submitted to severe thermomechanical solicitations [21]. The thermal expansion behavior of structural ceramics is critical for enduring high-temperature gradients and thermal shocks [22,27]. Fig. 10 displays the dilatometric curves of the studied materials in a technological temperature range (from room temperature up to 800 °C) which includes the molten aluminum processing or the combustion gas filtration.

For better comparison with other structural materials, apparent thermal expansion coefficients (α_{app}) were calculated, despite the observed behaviors were not strictly linear in the studied range; especially the ATZ15 material. α_{app} was evaluated with the following equation:

$$\alpha_{app} = \frac{(L_{800°C} - L_{25°C})}{L_0(800\ \ °C - 25\ \ °C)} \quad (5)$$

Were L_0 is the prismatic sample height and L_T corresponds to sample height at each temperature (T), employed in the vertical dilatometry test. α_{app} are shown in the inset of Fig. 10.

If we compare the obtained α_{app} values with the corresponding literature $\alpha_{1000\,°C}$ values for alumina (8×10^{-6} °C^{-1}), mullite ($\approx 4.5 \times 10^{-6}$ °C^{-1}), cordierite (1.4×10^{-6} °C^{-1}) and zircon (5×10^{-6} °C^{-1}) it can be corroborated that the developed materials present very low (and negative) α_{app} values. By comparing the three materials, we can see that α_{app} increases with the initial zircon content. In addition, it is worth pointing out that despite being a composite, the

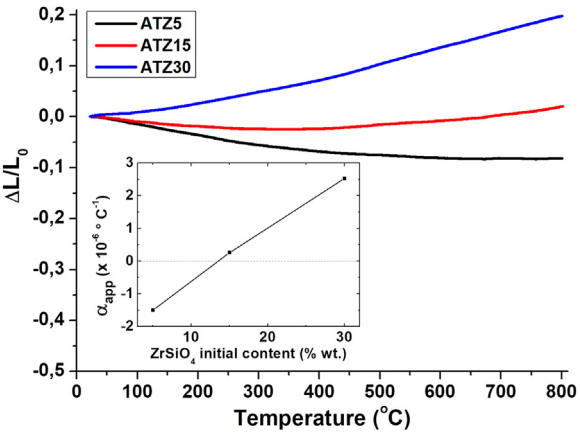

Fig. 10. Dilatometric analysis curves of the studied materials between 25 and 800 °C. Thermal expansion coefficients (α_{app}; RT-800 °C) are plotted in the inset as a function of the zircon content.

triplex composite ATZ30 material still has a low expansion.

4. Conclusions

- Aluminum titanate materials and aluminum titanate - mullite- zirconium titanate composite materials were successfully processed from fine commercial powders and characterized. This was achieved by zircon addition of stoichiometric alumina - titania mixtures. Zircon addition was the main processing variable explored.
- Developed phases were established, relatively dense ceramics were obtained and complex microstructures with multiphasic interlocked grains and an interconnected microcrack matrix that do not jeopardize the material integrity were identified.
- The thermal treatment was optimized, with complete conversion of aluminum titanate. Secondary chemical processes associated with zircon dissociation and new phase development was determined. A transient liquid mechanism was observed, which enhanced the material sintering that was also completed.
- Low or even negative thermal expansion behaviors were observed in the developed materials. This, together with the mechanical behavior detected, encourages structural applications with high thermomechanical solicitations.
- Zircon addition stabilized the unstable aluminum titanate phase, enhanced the sintering process, restricted microcrack development, and improved the mechanical properties of the ceramic material, but had a slight detrimental effect on the thermal expansion behavior of this material (α_{app} from -1.5–2.5×10^{-1} °C). The properties (P, D, σ_f, E_d, E_{st} and α_{app}) are directly (linearly) correlated with zircon proportion in the initial formulation.
- The ATZ30 material is in fact a triplex composite material with excellent thermomechanical properties and low porosity, 48 MPa flexural strength, low stiffness (E_d 35.51 GPa and E_{st} 7.66 GPa) and high sintering grade and low thermal expansion.
- With the gathered information a wide range of materials with specific thermomechanical properties can be obtained by only modulating the zircon proportion.

Acknowledgments

MAV and MFH acknowledge CONICET for the fellowships; this work was partially financed by ANPCyT (PICT-2016-1193) and CONICET (PIO CONICET-UNLA 2016–2018. No.: 22420160100023), and UNLP (2015–2018X-737). MSC is member of the CIC-PBA; MG, GS and NMR are members of the CONICET.

References

[1] M. Sternitzke, Review: structural ceramic nanocomposites, J. Eur. Ceram. Soc. 17 (1997) 1061–1082.
[2] K. Niihara, New design concept of structural ceramics, J. Ceram. Soc. Jpn. 99 (1991) 974–982, https://doi.org/10.2109/jcersj.99.974.
[3] P.H.C. Camargo, K.G. Satyanarayana, F. Wypych, Nanocomposites: synthesis, structure, properties and new application opportunities, Mater. Res. 12 (2009) 1–39, https://doi.org/10.1590/S1516-14392009000100002.
[4] W.P. Parks Jr., R.R. Ramey, D.C. Rawlins, J.R. Price, R. Van, Potential applications of structural ceramic composites in Gas Turbines, in. <http://dx.doi.org/10.1115/90-GT-251>, 1990.
[5] H.R. Thornton, J.E. Burroughs, Structural ceramic composites for aerospace applications, SAMPE J. 30 (1994) 41–46.
[6] R. Roy, D.K. Agrawal, H.A. McKinstry, Very low thermal expansion coefficient materials, Annu. Rev. Mater. Sci. 19 (1989) 59–81, https://doi.org/10.1146/annurev.ms.19.080189.000423.
[7] N.M. Rendtorff, S. Gómez, M.R. Gauna, M.S. Conconi, G. Suarez, E.F. Aglietti, Dense mullite-zirconia-zirconium titanate ceramic composites by reaction sintering, Ceram. Int. 42 (2016) 1563–1572, https://doi.org/10.1016/j.ceramint.2015.09.106.
[8] R. Bermejo, Y. Torres, C. Baudín, A.J. Sánchez-Herencia, J. Pascual, M. Anglada, L. Llanes, Threshold strength evaluation on an Al_2O_3-ZrO_2 multilayered system, J. Eur. Ceram. Soc. 27 (2007) 1443–1448, https://doi.org/10.1016/j.jeurceramsoc.2006.05.037.
[9] R. Bermejo, A.J. Sánchez-Herencia, L. Llanes, C. Baudín, High-temperature mechanical behaviour of flaw tolerant alumina-zirconia multilayered ceramics, Acta Mater. 55 (2007) 4891–4901, https://doi.org/10.1016/j.actamat.2007.05.005.
[10] N.M. Rendtorff, L.B. Garrido, E.F. Aglietti, Zirconia toughening of mullite-zirconia-zircon composites obtained by direct sintering, Ceram. Int. 36 (2010) 781–788, https://doi.org/10.1016/j.ceramint.2009.11.010.
[11] F.J. Parker, Al_2TiO_5-$ZrTiO_4$-ZrO_2 composites: a new family of low--thermal-expansion ceramics, J. Am. Ceram. Soc. 73 (1990) 929–932, https://doi.org/10.1111/j.1151-2916.1990.tb05138.x.
[12] I.J. Kim, H.C. Kim, Zero level thermal expansion materials based on $ZrTiO_4$-Al_2TiO_5 ceramics synthesized by reaction sintering, J. Ceram. Process. Res. 5 (2004) 308–312.
[13] F. Bakhshandeh, A. Azarniya, H. Madaah, S. Jafari, Are aluminium titanate-based nanostructures new photocatalytic materials? Possibilities and perspectives, J. Photochem. Photobiol. Chem. 353 (2018) 316–324, https://doi.org/10.1016/j.jphotochem.2017.11.043.
[14] I. YAMAI, T. OOTA, Low-thermal-expansion polycrystalline zirconyl phosphate ceramic, J. Am. Ceram. Soc. 68 (1985) 273–278, https://doi.org/10.1111/j.1151-2916.1985.tb15321.x.
[15] L. Stanciu, J.R. Groza, L. Stoica, C. Plapcianu, Influence of powder precursors on reaction sintering of Al_2TiO_5, Scr. Mater. 50 (2004) 1259–1262, https://doi.org/10.1016/j.scriptamat.2004.01.034.
[16] S.K. Jha, J.M. Lebrun, R. Raj, Phase transformation in the alumina-titania system during flash sintering experiments, J. Eur. Ceram. Soc. 36 (2016) 733–739, https://doi.org/10.1016/j.jeurceramsoc.2015.10.006.
[17] M. Nagano, S. Nagashima, H. Maeda, A. Kato, Sintering behavior of Al_2TiO_5 base ceramics and their thermal properties, Ceram. Int. 25 (1999) 681–687, https://doi.org/10.1016/S0272-8842(98)00083-2.
[18] C.-H. Chen, H. Awaji, Mechanical properties of Al_2TiO_5 ceramics, Key Eng. Mater. 336-338 II (2007) 1417–1419.
[19] Q. Zhang, W.H. Jiang, J.M. Liu, G. Feng, G.R. Xu, Low temperature synthesis of ultrafine Al_2TiO_5 powders by hydrolytic sol-gel method, Mater. Sci. Forum 848 (2016) 324–327, https://doi.org/10.4028/www.scientific.net/MSF.848.324.
[20] W.E. Lee, G.P. Souza, C.J. McConville, T. Tarvornpanich, Y. Iqbal, Mullite formation in clays and clay-derived vitreous ceramics, J. Eur. Ceram. Soc. 28 (2008) 465–471, https://doi.org/10.1016/j.jeurceramsoc.2007.03.009.
[21] I.J. Kim, Thermal stability of Al_2TiO_5 ceramics for new diesel particulate filter applications-a literature review, J. Ceram. Process. Res. 11 (2010) 411–418.
[22] I.J. Kim, Thermal shock resistance and thermal expansion behavior of Al_2TiO_5 ceramics prepared from electrofused powders, J. Ceram. Process. Res. 1 (2000) 57–63.
[23] S. Bueno, R. Moreno, C. Baudín, Reaction sintered Al_2O_3/Al_2TiO_5 microcrack-free composites obtained by colloidal filtration, J. Eur. Ceram. Soc. 24 (2004) 2785–2791, https://doi.org/10.1016/j.jeurceramsoc.2003.08.015.
[24] Y. Ohya, Z. Nakagawa, Measurement of crack volume due to thermal expansion anisotropy in aluminium titanate ceramics, J. Mater. Sci. 31 (1996) 1555–1559, https://doi.org/10.1007/BF00357864.
[25] A. Tsetsekou, A comparison study of tialite ceramics doped with various materials and tialite-mullite composites: microstructural, thermal and mechanical properties, J. Eur. Ceram. Soc. 25 (2005) 335–348, https://doi.org/10.1016/j.jeurceramsoc.2004.03.024.
[26] H.A.J. Thomas, R. Stevens, Aluminium titanate - a literature review. Part 1, Micro. Phenom., Br. Ceram. Trans. J. 88 (1989) 144–151.
[27] H.C. Kim, K.S. Lee, O.S. Kweon, C.G. Aneziris, I.J. Kim, Crack healing, reopening and thermal expansion behavior of Al_2TiO_5 ceramics at high temperature, J. Eur. Ceram. Soc. 27 (2007) 1431–1434, https://doi.org/10.1016/j.jeurceramsoc.2006.04.024.
[28] N.P. Padture, S.J. Bennison, H.M. Chan, Flaw-tolerance and crack-resistance properties of alumina-aluminum titanate composites with tailored microstructures, J. Am. Ceram. Soc. 76 (1993) 2312–2320, https://doi.org/10.1111/j.1151-2916.1993.tb07770.x.
[29] H. Schneider, J. Schreuer, B. Hildmann, Structure and properties of mullite—A review, J. Eur. Ceram. Soc. 28 (2008) 329–344, https://doi.org/10.1016/j.jeurceramsoc.2007.03.017.
[30] R. Torrecillas, J.M. Calderón, J.S. Moya, M.J. Reece, C.K.L. Davies, C. Olagnon, G. Fantozzi, Suitability of mullite for high temperature applications, J. Eur. Ceram. Soc. 19 (1999) 2519–2527, https://doi.org/10.1016/S0955-2219(99)00116-8.
[31] M. Hamidouche, N. Bouaouadja, C. Olagnon, G. Fantozzi, Thermal shock behaviour of mullite ceramic, Ceram. Int. 29 (2003) 599–609, https://doi.org/10.1016/S0272-8842(02)00207-9.
[32] Z. Malou, M. Hamidouche, B. Hocine, Thermal shock resistance of mullite obtained from Kaolin and tri-hydrated alumina, High Temp. - High Press. 47 (2018) 179–190.
[33] A. George, S. Solomon, J.K. Thomas, A. John, Characterizations and electrical properties of $ZrTiO_4$ ceramic, Mater. Res. Bull. 47 (2012) 3141–3147, https://doi.org/10.1016/j.materresbull.2012.08.018.
[34] B. Ganesh, C. Kumar, K. Ravichandran, P. Manohar, Synthesis and characterization of zirconium tin titanate ($Zr_{0.8}Sn_{0.2}TiO_4$), Int. J. ChemTech Res. 5 (2013) 2122–2129.
[35] A. Borrell, M.D. Salvador, V.G. Rocha, A. Fernández, A. Gómez, E. López-López, R. Moreno, ZrTiO4 materials obtained by spark plasma reaction-sintering, Compos. Part B Eng. 56 (2014) 330–335, https://doi.org/10.1016/j.compositesb.2013.08.046.
[36] E. López-López, R. Moreno, C. Baudín, Zirconium titanate: stability and thermal expansion, Boletin Soc. Esp. Ceram. Vidr. 50 (2011) 169–178, https://doi.org/10.3989/cyv.222011.

[37] E. López-López, C. Baudín, R. Moreno, I. Santacruz, L. Leon-Reina, M.A.G. Aranda, Structural characterization of bulk ZrTiO4 and its potential for thermal shock applications, J. Eur. Ceram. Soc. 32 (2012) 299–306, https://doi.org/10.1016/j.jeurceramsoc.2011.08.004.

[38] A. Bianco, G. Gusmano, R. Freer, P. Smith, Zirconium titanate microwave dielectrics prepared via polymeric precursor route, J. Eur. Ceram. Soc. 19 (1999) 959–963.

[39] M.F. Melo, J.S. Moya, P. Pena, A. De, Multicomponent toughened ceramic materials obtained by reaction sintering - Part 3 System ZrO_2-Al_2O_3-SiO_2-TiO_2, J. Mater. Sci. 20 (1985) 2711–2718, https://doi.org/10.1007/BF00553032.

[40] I.M. Low, D. Lawrence, R.I. Smith, Factors controlling the thermal stability of aluminum titanate ceramics in vacuum, J. Am. Ceram. Soc. 88 (2005) 2957–2961, https://doi.org/10.1111/j.1551-2916.2005.00518.x.

[41] N.M. Rendtorff, G. Suárez, E.F. Aglietti, Non isothermal kinetic study of the aluminium titanate formation in alumina-titania mixtures, Ceramica 60 (2014) 411–416, https://doi.org/10.1590/S0366-69132014000300013.

[42] M.R. Gauna, M.S. Conconi, S. Gomez, G. Suárez, E.F. Aglietti, N.M. Rendtorff, Monoclinic-tetragonal zirconia quantification of commercial nanopowder mixtures by XRD and DTA, Ceram. - Silik. 50 (2015) 318–325.

[43] R.D. Bonetto, P.E. Zalba, M.S. Conconi, M. Manassero, The Rietveld method applied to quantitative phase analysis of minerals containing disordered structures, Rev. Geológica Chile 30 (2003) 103–115, https://doi.org/10.4067/S0716-02082003000100007.

[44] H.M. Rietveld, A profile refinement method for nuclear and magnetic structures, J. Appl. Crystallogr. 2 (1969) 65–71.

[45] G. Roebben, B. Bollen, A. Brebels, H. Van, D.B. Van, Impulse excitation apparatus to measure resonant frequencies, elastic moduli, and internal friction at room and high temperature, Rev. Sci. Instrum. 68 (1997) 4511–4515, https://doi.org/10.1063/1.1148422.

[46] V. Polliotto, E. Albanese, S. Livraghi, P. Indyka, Z. Sojka, G. Pacchioni, E. Giamello, Fifty-Fifty Zr-Ti solid solution with a TiO_2-type structure: electronic structure and photochemical properties of zirconium titanate $ZrTiO_4$, J. Phys. Chem. C 121 (2017) 5487–5497, https://doi.org/10.1021/acs.jpcc.6b12892.

[47] A. Gajović, K. Furić, S. Musić, I. Djerdj, A. Tonejc, A.M. Tonejc, D. Su, R. Schlögl, Mechanism of $ZrTiO_4$ synthesis by mechanochemical processing of TiO_2 and ZrO_2, J. Am. Ceram. Soc. 89 (2006) 2196–2205, https://doi.org/10.1111/j.1551-2916.2006.00972.x.

[48] C.L. Wang, H.Y. Lee, F. Azough, R. Freer, The microstructure and microwave dielectric properties of zirconium titanate ceramics in the solid solution system $ZrTiO_4$-$Zr_5Ti_7O_{24}$, J. Mater. Sci. 32 (1997) 1693–1701, https://doi.org/10.1023/A:1018563630617.

[49] K. Niihara, New design concept of structural ceramics. Ceramic nanocomposites, J. Ceram. Soc. Jpn. 99 (1991) 974–982, https://doi.org/10.2109/jcersj.99.974 (Nippon Seramikkusu Kyokai Gakujutsu Ronbunshi).

[50] M. Kachanov, Elastic solids with many cracks and related problems, in: J.W. Hutchinson, T.Y. Wu (Eds.), Adv. Appl. Mech. Elsevier, 1993, pp. 259–445, , https://doi.org/10.1016/S0065-2156(08)70176-5.